An evaluation of offshore wind power production by floatable systems: a case study from SW Portugal

Pacheco, A.[1*], Gorbeña, E.[1], Sequeira, C.[1], Jerez, S.[2]

[1]MORE-CIMA/Universidade do Algarve, Edifício 7, Campus de Gambelas Faro, 8005-139, Portugal, ampacheco@ualg.pt, egeisenmann@ualg.pt, cdsequeira@ualg.pt; [2]Instituto Dom Luiz, Faculdade de *Ciências*, Universidade de Lisboa, Campo Grande, Edifício C1, 1749-016 Lisboa, Portugal, sjrodriguez@fc.ul.pt

Abstract

The challenge for floating offshore wind structures is to reduce costs. The industry needs a wind turbine support solution that can be fabricated and deployed from existing shipyards and port facilities, while investors need accurate estimations and forecasts of wind resources and quantified information on the inherent variability in wind power generation. This paper merges hindcast model data with observed in situ data to characterize the wind resource potential off the SW coast of Portugal. The validation procedure adopted allows an estimation of the coefficient used for power-law extrapolation of the wind measurements and a reduction in the uncertainty of the power density calculations. Different types of turbine model are compared and site metocean characteristics are examined as a basis for choosing between existing wind floatable solutions. The calculations using four different wind turbine models indicate a preferable installed capacity of 3–4 MW for a hub height of 90–120 m (i.e., representing the best capacity factor and load hours). There is a consistent difference in power density of about 20% from a location 5 nautical miles (NM) offshore to one 10 NM offshore, which represents an increment of 20%–25% in energy production depending on the particular wind turbine capacity factor.

Keywords: Floatable offshore wind solution, Wind resource estimation, Wind energy production, SW Portugal, Wind Farm Lagoa Funda

1. Introduction

Economic growth and increasing human demands are driving the growing world energy consumption. Because of rising prices for both oil and natural gas, reduced fuel reserves, and obligations to reduce CO_2 emissions to avert climate change, the use of alternative energy sources is both financially unavoidable and environmentally preferable. Hence, the generation of renewable energy has become one of the most relevant endeavours for research in the energy industry.

Europe, the US, and Japan have the potential to tap into an exceptional renewable energy resource from as yet unexploited offshore wind along their coastlines. The world's first offshore wind project was installed off the coast of Denmark in 1991. Since that time, commercial-scale offshore wind power facilities have been operating in shallow waters around the world, mostly in Europe. In 2013, 2080 wind turbines were installed and connected to the grid, producing a combined total of 6562 MW from 69 offshore wind farms in 11 European countries [1]. In terms of installed capacity, the average offshore wind farm size was ~485 MW in 2013 but has since decreased to 368 and 338 MW in 2014 and 2015, respectively. These installations are located at water depths of ~20 m and ~30 km offshore and are fixed technologies, of which 78.8% are monopiles, 10.4% are gravity structures, 4.7% are jackets, 4.1% are tripods, and 1.9% are tripiles. Once completed, the 12 offshore projects under construction will increase the installed capacity by a further 3 GW, bringing the cumulative capacity in Europe to 9.4 GW [2].

Most future offshore wind farms will present greater generation capacity and will move into deeper waters and further from the coast, and therefore other technologies more suited to greater water depths will be required. This is the main reason why research in coming years will be focused on offshore energy generation using floating systems. As an example, the electricity production from floating turbines deployed in sea areas at water depths of 60–120 m is targeted to meet 50% of Europe's electricity needs by 2050 [2].

Newer wind turbine and foundation technologies are being developed so that the wind power resource at deep-water sites can be exploited in the future (Fig. 1). Each of these concepts has its particular advantages and disadvantages (Table 1). The International Energy Agency (IEA) has presented a range of scenarios for the scale of offshore wind power deployment that will be required to avoid global warming above the 2 °C target defined by the United Nations Framework Convention on Climate Control (UNFCCC) [3]. The IEA recommends that governments internationally should target achieving an offshore wind installed capacity of 118 GW by 2020 increasing to 1142 GW by 2050. The most significant potential benefit will be the reduction in CO_2 emissions through the avoidance of hydrocarbon-based power generation. Globally, electricity production accounted for 42% of the world's CO_2 emissions in 2014, or 15.4 trillion tonnes. If the regions with suitable water depths (60 to 120 m) in Europe, the US, and Japan were to be exploited by floating offshore wind power generation devices, then this would equate to 650 GW of installed capacity, which, when in operation, would avoid 0.7 trillion tonnes of CO_2 emissions [2]. Thus, having an effective platform technology for exploiting wind in areas of deep water will give access to a market that is predicted by the IEA as having the most growth potential over the next two decades.

A potential barrier to developing offshore wind energy is the general lack of accurate information in most offshore areas about the wind resource characteristics and external metocean design conditions at the heights and depths relevant to wind turbines and their associated structures and components (Fig. 2). Knowledge of these conditions enables the appropriate design basis for wind turbine structures and components to be specified so that they can withstand the loads expected over a project's lifetime. However, metocean data are sparse in potential development areas and, even when available, do not include the detail or quality required to make informed decisions. Therefore, there is a critical need to improve the characterization of metocean conditions to facilitate future offshore wind energy developments. Climate model outputs, either global reanalyses or higher-resolution hindcast products, can help to overcome such a limitation by providing physically consistent, homogeneous, spatially dense information about weather and climate conditions over areas with insufficient observations [4,5].

Portugal has a coastal shelf with water depths ranging from 25 to 200 m with low slopes (~3%) and a moderate offshore wind resource. The geographical features of the Portuguese coast are therefore favourable to the implementation of offshore systems, particularly for floating technologies, which are expected to be commercially available in Europe from 2020. The first step in the development of an offshore wind resource sector is the characterization of wind potential through the use of mapping and the identification of macro-regions with wind potential off the Portuguese coast. The present study has two principal objectives: (1) to combine wind model data with wind turbine data to assess the wind resource potential in SW Portugal, thus characterizing the area for offshore wind energy resource exploitation; and (2) to perform an analysis of the metocean characteristics of the site and discuss the arguments relevant to choosing options from existing wind energy floatable solutions.

2. Study area

The stretch of the SW Portuguese coastline between Sagres and Aljezur (Fig. 3), hereafter referred to as the "Sagres Area", has a relatively narrow continental shelf (10–30 km wide) that dips moderately towards the continental slope and has low sediment cover [6]. In particular, the Sagres Area descends abruptly to depths of over 1000 m at the continental slope. Under the terminology of the European Union Water Framework Directive, the Sagres Area is classified as a mesotidal, moderately exposed Atlantic coastal type.

The tidal conditions are characterized by a semidiurnal regime, with a tidal cycle of approximately 12 hr 25 m, and mesotidal amplitudes that can range from ~1 m during neap tides to more than 3.5 m during spring tides. Storm surge has been shown to increase water levels up 0.75 m, but only under extreme conditions, as in 99% of occurrences storm surge values are below 0.5 m [7]. The coast is directly exposed to North Atlantic swell and storms. The area therefore experiences a high-energy wave climate, with the mean offshore significant wave height (H_s) ranging between 1.5 and 2 m and average peak wave period (T_P) between 9 and 13 s for summer and winter periods, respectively [8]. Waves approach from the northwest to west throughout the year. The prevailing winds blow from the N to NW (>50% annual frequency), and the mean maximum wind velocities are ~22 kmh^{-1}.

The part of the Sagres Area closer to Cabo São Vicente is dominated by the interaction of two weather regimes. The first regime occurs during early spring to late summer, when the west coast of Portugal is subject to northerly winds, a consequence of the typical synoptic configuration consisting of the Iberian thermal low plus the Azores high, which promotes upwelling events. The second regime occurs along the south coast of Portugal and is characterized by the presence of a warmer and more saline coastal counter-current over the continental shelf, which develops whenever there is a relaxation of the wind that sustains the upwelling [9]. The annual cycle of sea surface temperature, wind vectors, and

Ekman transport for the SW Portuguese coast shows that this coastal stretch is affected by northerly winds throughout the year [10]. It is during the months of April–September that the wind and associated Ekman transport are strongest (>600 $kgm^{-1}s^{-1}$). From November to March, the southward drift of the Azores High affects the wind regime, and consequently the wind stress is reduced and the Ekman transport falls to an annual minimum in January (<50 $kgm^{-1}s^{-1}$).

3. Methods

3.1. **Wind model and in situ data**

The distribution of wind speed and direction and their variation over short time scales are primary concerns for the development and operation of offshore wind energy. Wind resource can be described by mean velocity (speed and direction) and turbulence intensity. These conditions characterize the potential energy available at a site, influence turbine selection, drive the balance of the designed plant, and affect project construction and operational strategies. Measurements of wind speed and direction are preferred across the entire wind turbine operating height, with a priority on hub height. Current industry practices employ a combination of direct and remote sensors to observe wind conditions.

The wind model data used for the preliminary resource assessment of Sagres Area were retrieved from a 49 year hindcast simulation performed with the Fifth-Generation Pennsylvania State University – National Center for Atmospheric Research Mesoscale Model (MM5) [9], which encompasses the period 1959–2007 covering the whole Iberian Peninsula with a 10 km spatial resolution. The simulation was driven by the European Centre for Medium-Range Weather Forecast (ECMWF) ERA40 reanalysis [13] up to 2002 and analysis data afterwards, up to 2007, and provides hourly records of surface winds at a height of 10 m for the entire simulated period. This simulated dataset has been previously used and validated against observations in several studies focused on a variety of topics [14–20]. Here, hourly wind speed and direction series for three locations within the Sagres Area (Fig. 3) were extracted: the onshore Aeolian Park of Lagoa Funda (APLF, 37.145184°N, 8.9018326°W), 5 nautical miles (NM) offshore of the APLF at ~50 m depth (37.138325°N, 9.0171232°W), and 10 NM offshore of the APLF at ~100 m depth (37.131348°N, 9.1323900°W).

The wind profile of the atmospheric boundary layer is generally logarithmic in nature and is best approximated using the log wind profile equation that accounts for surface roughness and atmospheric stability:

$$U = \frac{u_*}{k}\left[\ln\left(\frac{z}{z_0}\right) - \psi_m(\zeta)\right] \quad (1)$$

where U is the mean wind speed (ms^{-1}) at height z (m); u_* is the friction velocity (ms^{-1}); k is the Von Kármán constant (~0.41); and $\psi_m(\zeta)$ is the integrated stability function for momentum [21], where $\zeta = \frac{z}{L}$, with L representing the Obukhov length scale, given by:

$$L = -\frac{{u_*}^3}{k\frac{g}{\Theta_0}\overline{w\theta}} \quad (2)$$

where g is gravitational acceleration (ms^{-2}), Θ_0 is the surface temperature (° C), and $\overline{w\theta}$ is the kinematic heat flux ($Jm^{-2}s^{-1}$). The Obukhov length is obtained from sonic anemometers using eddy-correlation techniques. The dimensionless height ζ is used as a stability parameter ($\zeta < 0$ indicates unstable, $\zeta > 0$ stable, and $\zeta = 0$ neutral conditions) [22].

However, when surface roughness or stability information is not available, the wind profile power-law relationship is often used as a substitute for the log wind profile, especially in wind power assessments where wind speeds at the height of a turbine must be estimated from near-surface wind observations (~10 m as in this case). The wind profile power-law relationship is:

$$U = U_R\left(\frac{z}{z_R}\right)^{\alpha} \quad (3)$$

where U is the mean wind speed (ms^{-1}) at height z (m), and U_R is the reference wind speed (ms^{-1}) at height z_R (m). The exponent α is an empirically derived coefficient that varies between 0.04 and 0.60 depending upon the stability of the atmosphere, and represents physical information about atmospheric conditions in a single parameter [23]; the exponent fits data well in the first few metres of the atmospheric boundary layer [24]. A wind speed shear exponent of ~0.1 has been used in previous studies [25, 27] for extrapolating offshore wind speeds using a power law at a height of 90 m. Thus, in the present study and for an initial assessment of the wind resource at the APLF, a value for α of 0.1 is used for a hub height of 80 m. The value is then adjusted using a validation procedure by comparing the results of the model with those of the meteorological mast station located inside the APLF (refer to sub-section 3.3 for further details).

3.2. **Wind statistics and the Weibull distribution**

It is essential for the wind industry to properly describe the variation in wind speeds. Wind turbine designers need this information to optimise the design of their turbines, so as to minimise generation and maintenance costs. To calculate the mean power from a wind turbine over a range of mean wind speeds, a generalised expression is needed for the probability density distribution. An expression that gives a good fit to wind data is known as the Weibull distribution. The Weibull distribution is a two-parameter function commonly used to fit the wind speed frequency distribution. The probability density function (PDF) of the Weibull distribution is given by

$$f(U) = \frac{k}{c}\left(\frac{U}{c}\right)^{k-1} e^{-\left(\frac{U}{c}\right)^{k}} \qquad (4)$$

where $f(U)$ is the probability of wind speed U, k is the dimensionless shape parameter, and c is the scale parameter in units of wind speed. Once the c and k parameters are known, the moments and percentiles of the wind speed distribution may be computed.

The Cumulative Distribution Function (CDF) of the Weibull distribution is given by

$$F(U) = 1 - e^{-\left(\frac{U}{c}\right)^{k}} \qquad (5)$$

This family of curves has been shown to give a good fit to measured wind speed data [28] by providing a convenient representation of the wind speed for wind energy calculation purposes [29]. Different methods have been proposed to estimate Weibull parameters, which have been compared in the literature several times, but with different results and recommendations [29, 30]. In the present study, the Weibull parameters are determined using the maximum likelihood method [29] and then applied to estimate the energy density, that is, the wind power resource that can be harnessed using wind turbines. The Weibull distributions are determined for the three sites and for each month. The vertical mean speed power-law profile (Eq. 3) is used to extrapolate the wind speed to the wind turbines' hub heights.

3.3. **Observational data and validation procedure**

Wind resource estimates are characterized by various degrees of uncertainty that could lead to highly misleading results. An accurate estimation of wind fields requires reliable datasets so that wind power assessment can be performed with reduced uncertainty. Most often, risk-based financial models, on which wind project investments are based, are strongly dependent upon these uncertainties [30]. In the present study, the hindcast dataset is directly compared with an in situ observational wind database at hub height from the station located inside the APLF. The station is equipped with wind velocity and directional sensors placed at a height of 80 m, and recorded wind speed and directional data are available for 5 minute intervals from 2003 to 2007. Although the data period is long and high frequency, the measurements from the sensors have registered several anomalies that have significantly reduced the data coverage (Table 3). Careful analysis of the data allowed erroneous values and any systematic errors in the measurements to be eliminated. Two periods were considered: from January 2003 until December 2005 and from September 2006 to August 2007, comprising a total of 4 years of data for model validation. Because no temperature data are available, the comparison between the model and station data is herein used to estimate the α exponent in Eq. 3 and to reduce the uncertainty of the power estimates.

3.4. **Quantification of the offshore wind resource**

The power density accordingly to the Weibull PDF is given by

$$P = \frac{1}{2}\rho \int_0^N U^3 f(U) dU \qquad (6)$$

where ρ is the air density (kgm^{-3}) at a certain height and temperature (e.g. ~1.226 kgm^{-3} at mean sea level and 15 °C).

To estimate the power and energy output from the different turbine devices, the Weibull distributions are combined with the power curve, that is, each interval of wind speed is multiplied by the probability of that wind speed interval (from the Weibull curve) and by the value from the power curve (P_T) supplied by each wind turbine manufacturer. The mean (or average) power output is obtained by

$$P_{mean} = \sum P_T(U) f(U) \qquad (7)$$

Multiplying the power by 365.25 and by 24 (the number of hours in a year), the total energy output for an average year is obtained (E_{out} in $kWhyear^{-1}$). The wind turbine parameters analysed in this study were selected based on the different wind turbines normally used for offshore wind energy farms (Table 2). A turbine availability of 100%

is assumed (i.e., no losses due to problems such as down time, icing, gearbox losses, transformer losses, or farm effects). The capacity factor (C_F) is obtained by dividing E_{out} by the turbine's rated output for the same period of time, and the full load hours can be determined, namely, the theoretical number of hours that the wind turbine has to run at full load in order to produce the annual yield (i.e., full load hours = capacity factor * number of hours in a year).

4. Results

The wind power time series obtained for the location of the APLF is presented in Fig. 4A and is based on the hourly estimates of velocity from the 49 year hindcast model data as described in sub-section 3.1. The power computations were determined based on the velocity distribution from the Weibull PDF function (Fig. 4B) by extrapolating the model velocity results to a height of 80 m and adopting a value for the α coefficient of 0.1 (Eq. 3). The Weibull c parameter is 7.59 ms^{-1} and the k parameter is 2.39 (Table 4). The mean velocity (U_{mean}) based on the long-term distribution is 6.74 ms^{-1} with a standard deviation (σ) of 2.98 ms^{-1} and a maximum velocity (U_{max}) of 25.56 ms^{-1}. The boxplot of monthly wind distribution (Fig. 4C) allows the variability in wind intensity throughout the year to be characterized. In Fig. 4C, for each month, the central horizontal mark (red line) in the box represents the median value, the top and bottom edges of the box respectively represent the 75th and 25th percentiles, the dashed black line above and below the box represents sample variability, and the horizontal red marks beyond the dashed line represent outlier values. Points are defined as outliers if they are larger than $q_3 + w(q_3 - q_1)$ or smaller than $q_1 + w(q_3 - q_1)$, where $w = 1.5$ and q_1 and q_3 are the 25th and 75th percentiles, respectively. The wind rose (Fig. 4D) allows an assessment of the wind regime predominance in each directional partition and the probability of occurrence of each of them (as a percentage frequency) with respect to the total amount. The wind rose frequency for the APLF shows that the most probable winds come from the NW to N. Their probability of occurrence is approximately ~35%, although maximum wind velocity values are more frequent from the S to SE (~15% occurrence probability).

To validate the results and to perform accurate resource estimations for the offshore area (i.e., at sites 5 and 10 NM offshore the APLF), the velocity estimates from the model time series (i.e., Fig. 4) were compared with an in situ observational wind database from the station located inside the APLF (5 minutes frequency; 4 years data measured at a hub height of 80 m). Those results are presented in Fig. 5 and are summarised in Table 4. A preliminary comparison between Figs. 4 and 5 reveals the following: the observed power estimates exceed those obtained using the model; the Weibull PDF has c and k parameters for the APLF station data of 6.70 ms^{-1} and 2.36, respectively (Table 4); a similar trend in the boxplot of wind intensity variability (Fig. 5C), where the median wind velocity is also higher in July (~7.5 ms^{-1}) and with higher variability; the outliers are more frequent during the winter months, which are generally characterized by lower velocities and high variability; and, finally, the wind rose for the APLF station shows higher frequencies of N–NW winds (~35%), as well as a ~15° gap in the directional data (i.e., N0°–N15°).

Overall, the model reasonably represents the annual trends obtained from the in situ data, but the modelled velocities are higher, a well-known problem that is attributed mainly to a misrepresentation of frictional forces in the model [12]. This misrepresentation results in an overestimation of the wind power at the APLF location (U_{mean} = 5.91 ms^{-1}; σ = ±2.63 ms^{-1}; U_{max} = 25.4ms^{-1}). Thus, if trends are well represented, the problem is not the use of the model data but, rather, the extrapolation of the wind velocities from the surface to the hub height, that is, the influence that the α parameter value has on the final computations. Reducing the α parameter to half (i.e., ~0.05) and performing similar computations results in c and k parameters of 6.84 ms^{-1} and 2.39, respectively, and the resultant yearly U_{mean} is 6.08 ms^{-1} (σ = ±2.68 ms^{-1}), that is, almost a match between the observed and model data for the Weibull PDF while maintaining similar data trends (e.g., the monthly intensity of wind speeds and directions).

On the basis of the above estimation of the α parameter, and using the model velocity wind speed data extracted from grid points at 5 and 10 NM offshore, the wind velocity histograms and Weibull probability density and cumulative functions were produced, as well as the monthly wind velocity distributions and wind rose directional charts (Figs. 6 and 7, respectively). The Weibull PDFs (Figs. 6A and 7A) indicate that c = 7.81 ms^{-1} and 8.09 ms^{-1}, respectively, for 5 and 10 NM, while k ~ 2.45 and 2.49, respectively (Table 4). The U_{mean} values are 6.94 ms^{-1} and 7.18 ms^{-1}, with σ values of ±2.97 and ±3.12 ms^{-1}, respectively (Table 5). The mean regime for each site is presented in Figs. 6B and 7B through a Weibull CDF, a probability plot showing the relationship between a specific wind speed value (U) and its probability ($F(U)$), where $F(U)$ indicates the probability that the wind velocity is equal to or lower than U. These are required data for a possible wind farm; for example, a wind speed of 10 ms^{-1} can be considered a large mean value for offshore wind energy and has an associated probability in the CDF of ~0.8 for both sites. The monthly distribution of U (Figs. 6C and 7C) and wind rose frequency (Fig. 6D and 7D) for both offshore sites are similar to and consistent with the APLF site.

To estimate the wind power (Eq. 7) and energy output generated by a specific wind turbine device at a given site over a defined period, the power characteristics of the turbines (Table 2) were integrated with the probabilities of different wind velocities expected at each of the offshore sites (Figs. 6 and 7). The integration was performed at a 0.1 ms^{-1} interval, and the results are presented in Fig. 8 and summarised in Table 5.

5. Discussion

Several wind modelling methodologies are now being used for estimating wind power resources and wind energy output at different spatial and temporal scales [31–32]. A fundamental limitation of most of these modelling techniques is the calibration with available in situ data, which can result in significant differences in wind energy estimates and therefore in technical and economic predictions [33].

The power output and cost effectiveness of a wind turbine are strongly influenced by the mean wind speed to which it is subjected, and therefore wind speed needs to be accurately determined. The initial α exponent value (i.e., 0.1) was chosen based on the validation experience with the updated offshore wind maps for the US and is within the range of 0.08 to 0.14 reported in other analyses for the same region [25]. In a similar study of the creation of a wind resource map for the Iberian Coast using remotely sensed data, a power law was also used with a shear exponent value α of 0.1 [27,34]. A direct comparison between model data and in situ data measured at the SW coast of Portugal in the present study reveal that α is around 0.05, and therefore this value should be adopted for using a power-law function to estimate wind velocities at hub height if there are no data on atmosphere variability throughout the analysed period. The same α shear exponent value was obtained at Santander (Spain) by fitting Eq. 3 to 20 years of hourly measurements obtained at different heights (i.e., 15, 40, 75, and 110 m [35]).

The offshore wind resource assessment results indicate that both the 5 and 10 NM sites are characterized by mean wind speed values of <8.0 ms^{-1}. Higher variability occurs during the autumn–winter months (October to March), but maximum wind velocities occur during the spring–summer months, although generally with less variability. The highest median value occurs in July (~7.5 ms^{-1}), which, although having a lower number of residuals, is also characterized by a relatively high variability in wind intensity. The US National Renewable Energy Laboratory (NREL) [26] has defined a wind power scale to classify the suitability of a region for a wind project (Table 6), in which a site with a wind mean power density of 150 Wm^{-2} (Class 3) or above is considered suitable for most utility-scale wind turbine applications. On the basis of the NREL classification, the Sagres Area is rated as Class 5, that is, U_{mean} ~ 6.7–7.2 ms^{-1} (Table 4).

From an energy point of view, and taking into consideration the four analysed wind turbine devices, the Siemens SWT 3.6 MW is the most suitable turbine for the wind flow characteristics for both the 5 and 10 NM locations. This device presents the best capacity factor and a similar energy production when compared with the increment of 1.4 MW of installed capacity of the AREVA M5000 wind turbine. The energy production of the Siemens turbine ranges from 11.4 to 14.0 $GWhyear^{-1}$ for a single unit, corresponding to 3154 and 3900 $hyear^{-1}$ equivalent hours at full capacity if placed at 5 and 10 NM, respectively.

As a consequence of using α = 0.05, the results show that hub height has a moderate effect on the power density (P) availability, with the availability for a hub height of 126 m compared with one of 66 m being up to 3.5% and 7.0% higher at the 5 and 10 NM locations, respectively. There is a consistent difference in the power density of about 20% between the 5 and 10 NM locations, which represents a 20% increase in energy production (E_{out}) for the Vestas V66 and SWT 3.6 turbines and 24% for the Areva M5000 and Repower 6.2M turbines. Compared with the other turbines, C_F is higher for the SWT 3.6 for both the 5 and 10 NM locations: 0.36 and 0.45, respectively, resulting in a higher value of full load hours. There are minor differences in terms of energy production between the SWT 3.6 and Areva 5000 devices, and opting for Repower 6.2 generates an overall increment of 24% in the total energy production, with values of C_F of 0.24 and 0.36 for the 5 and 10 NM locations.

Given the characteristics of the Portuguese continental shelf, it is expected that floating platforms for harnessing wind will be installed offshore and in waters greater than 50 m deep. Floating platforms attempt to meet the requirements of high stability and low motions in waves by adopting one of three established solutions from the oil and gas industry (Fig.1 and Table 1), namely, semi-submersible platforms, deep-draught mono-spar platforms, and tension-tethered platforms (TTPs). The dynamics of floating offshore wind turbines involve significant coupling between the aerodynamics of the wind turbine and the hydrodynamics of the platform. The motions from the turbine, waves, and the moorings all contribute to the overall dynamic response of the system.

The US-based DeepCWind consortium tested three platforms coupled with a scaled device of the NREL 5 MW wind turbine [36]. The setup included a TTP, a semi-submersible, and a spar. The full results of the study were made available by Robertson et al. [37]. Another comparative study was made with the joint efforts of Osaka Prefecture, Yokohama National, Nihon, and Osaka universities. Contributors provided their platform design, to be coupled with a 5 MW scaled turbine and a tower of 90 m. A TTP, two semi-submersibles, and a SPAR type platform were evaluated. The comparative results of that study were discussed by Nihei et al. [38], and the findings concur with DeepCWind studies with respect to platform characteristics, namely, that waves are the main driver of platform motions as opposed to wind; the TTP provides stability in pitch, roll, and heave motions; the spar shows the highest acceleration values in most wave–wind regimes; and the semi-submersible delivers the highest surge motion overall but half of the pitch/roll/heave compared with the spar.

As an example, Principle Power's Windfloat project located offshore the NW coast of Portugal (3.1 NM offshore at 40–50 m depth) makes use of a triangular semi-submersible platform to sustain a Vestas 2 MW turbine (hub height ~90 m). The platform has low motion under waves but needs to be sufficiently large to achieve the required stability (38 m and 53 m between vertices at the surface and base, respectively). This platform can be port assembled, does not require special vessels for towing (as it behaves as a hydrostatically stable structure), and uses standard mooring equipment. In fact, almost all offshore wind turbines are tri-blade horizontal-axis wind turbines, and the average wind turbine capacity is between 3 and 4 MW. Virtually all current developments in floating platforms are designed for ~2.5 MW turbines. While larger blades increase each turbine's swept area, the towers on which those turbines are installed must also be increased to accommodate the required blade-tip clearance between the turbine and the sea surface. The same principle applies to the platform so as to sustain larger overturning movements and to maintain overall stability under wave loads.

The Sagres Area is located ~56 NM south of the Port of Sines (37°57′N, 08°53′W), one of the most important deep-water ports in Portugal. Although deep, the port's facilities and the characteristics of the nearby offshore zone do not allow the assembly of most typical TLP platforms. The Sagres Area is bedrock dominated, and high-energy wave conditions are relatively frequent (H_{so} > 3 m for 10% of an average year [8]). Although spar-buoys are easy to fabricate and provide good stability, they also require a large draft, which creates logistical challenges during assembly, transportation, and installation, especially at high-energy sites. Solutions that involve mating the heavy wind turbine to its floating foundation structure at sea are considered high risk, as such offshore operations are complex, risky, weather dependent, potentially hazardous, and very expensive. In contrast, large-draft platforms limit the ability to tow the structure back to port for repairs on major components such as gearboxes and generators. The greatest advantage of semi-submersible platforms appears to be the building of a heavy structure to provide buoyancy and stability.

The industry needs a solution that is physically more compact so that a new wind-supporting structure and turbine can be built using existing ship or offshore construction facilities and which avoids the need for complex and costly assembly operations at the exposed wind farm site. It is therefore unlikely that in the near future, floatable offshore wind turbine capacity would be greater than 4 MW, and the flexible application of semi-submersible platforms appears to be an ideal solution for most markets with simple catenary mooring systems (e.g., the Windfloat project, which has been shown to be able to utilise existing commercial wind turbine technology). However, other concepts are being designed combining both semi-submersible and spar concepts to offer a solution with relatively small water plane area so that the natural frequencies in heave fall outside the wave frequencies, thereby allowing the device to cope with extreme wave conditions.

6. Conclusion

This paper presents a reliable wind power assessment of the offshore Sagres Area (SW Portugal) based on a long-term evaluation of the wind frequency distribution. The hindcast dataset used in the wind assessment study was validated with an in situ observational wind database at hub height from a meteorological station located inside an onshore coastal wind farm. The comparison between the model and observed data enabled the power-law wind shear exponent α to be corrected, preventing overestimation of the wind resource. The offshore Sagres Area has the potential for offshore wind exploitation, and the calculations using four different turbine devices point to an output of 3–4 MW for a hub height of 90–120 m (i.e., the best capacity factor and load hours). There is a consistent increment in power density of about 20% from the 5 to the 10 NM offshore location, which represents an increment of 20%–25% in energy production.

The current high cost of floating wind structures is a barrier to the exploitation of deeper water sites for wind energy exploitation. The reason for the higher costs of floating foundations is that the current solutions being offered are physically very large so as to achieve sufficient platform stability to support high-capacity (≥6 MW) wind turbines. These large platforms dictate the need for highly specialised construction docks, which limits the number of facilities where units can be easily built and launched. The advantages and disadvantages of different floatable platform solutions have been discussed herein based on the site characteristics and the proximity to port and dock infrastructures for the provision of logistical support during the construction and operation phases. The analysis indicates that semi-submersible platforms with simple catenary mooring systems can be easily deployed from existing port infrastructures. Future investigations will be oriented towards establishing the optimum siting and layout for a wind energy development off the SW coast of Portugal. Those investigations will focus on other variables for selecting suitable wind farm locations, including detailed wave and current statistics, environmental issues, the distance to shore and to potential onshore grid connection points, and the voltage capacity of National Grid transmission lines.

Acknowledgments

The paper is a contribution to the SCORE project, funded by the Portuguese Foundation for Science and Technology (FCT – PTDC/AAG-TEC/1710/2014). André Pacheco was supported by the Portuguese Foundation for Science and Technology under the Portuguese Researchers' Programme 2014 entitled "Exploring new concepts for extracting energy from tides" (IF/00286/2014/CP1234). Sonia Jerez was supported by the Portuguese Foundation for Science and Technology Investigator Programme 2015 (IF/01142/2015). The authors acknowledge IberWind for supplying the wind data measurements and turbine production data for the Aeolian Park of Lagoa Funda located in the Sagres Area.

Notation

A_T	Turbine sweep area [m^2]
α	Power-law coefficient [-]
c	Weibull scale parameter [ms^{-1}]
CDF	Weibull Cumulative Distribution Function
C_F	Capacity factor [-]
C_p	Turbine efficiency [-]
E_{out}	Total energy output for an average year [kWhhryear^{-1}]
$f(v)$	Probability of wind speed (v)
$F(v)$	Cumulative distribution of wind speed (v)
g	Acceleration of gravity [ms^{-2}]
H_s	Significant wave height [m]
H_{so}	Mean offshore significant wave height [m]
K	Von Kármán constant [-]
k	Weibull dimensionless shape parameter [-]
L	Obukhov length scale [m]
NM	Nautical mile(s) [~1.852 km]
Θ_0	Surface temperature [° Celsius]
P	Mean power density [Wm^{-2}]
PDF	Weibull Probability Density Function
P_{mean}	Mean (or average) power output [Wm^{-2}]
P_T	Mean power extracted by a turbine [Wm^{-2}]
ρ	Air density [kgm^{-3}]
T_p	Peak period [s]
U	Mean wind speed [ms^{-1}]
U_{max}	Maximum wind speed [ms^{-1}]
U_R	Wind speed [ms^{-1}] at height z_R [m]
u_*	Friction velocity [ms^{-1}]
$\overline{w\theta}$	Kinematic heat flux [Jm^{-2}s^{-1}]
z	Height [m]
z_0	Reference length [m]
z_R	Reference height [m]

References

[1] European Wind Energy Association report (2013). "Deep Water – The Next Step for Offshore Wind", 15 pp.

[2] IEA (2013). "Wind Energy Roadmap", 63 pp.

[3] European Wind Energy Association report (2014). "The European Offshore wind industry – key trends and statistics 2013", 22 pp.

[4] Tapiador, F. J. (2009). Assessment of renewable energy potential through satellite data and numerical models. Energy & Environmental Science 2(11): 1142–1161.

[5] Jerez, S., Thais, F., Tobin, I., Wild, M., Colette, A., Yiou, P., Vautard, R. (2015). The CLIMIX model: A tool to create and evaluate spatially-resolved scenarios of photovoltaic and wind power development. Renewable and Sustainable Energy Reviews, 42, 1–15.

[6] Loureiro, C. (2012). Geomorphology and Morphodynamics of Embayed Beaches in Contrasting Environments. PhD Thesis, 189 pp.

[7] Gama, C., Dias, J.M.A., Ferreira, Ó., Taborda, R., 1994. Analysis of storm surge in Portugal, between June 1986 and May 1988. Proceedings of Littoral'94, EUROCOAST, Lisboa, Portugal. pp. 381–387.

[8] Costa, M. and Esteves, R., 2010. Clima de agitação marítima na costa oeste de Portugal Continental. Proceedings of XI Jornadas Técnicas de Engenharia Naval — O Sector Marítimo Português. Edições Salamandra, Lisboa, Portugal, 413–426.

[9] Relvas, P., Barton, E.D. (2005). A separated jet and coastal counterflow during upwelling relaxation off Cape São Vicente (Iberian Peninsula). Cont. Shelf Res. 25(1): 29–49.

[10] Sánchez, R., Relvas, P. (2003). Spring–summer climatological circulation in the upper layer in the region of Cape St. Vincent, Southwest Portugal. ICES J. Mar. Sci. 60(6):1232–1250.

[11] Grell, G. A., Dudhia, J., Stauffer, D. R. (1994). A description of the fifth-generation Penn State/NCAR mesoscale model (MM5). NCAR Tech. Note NCAR/TN-398 + STR, Boulder, CO, 117 pp.

[12] Lorente-Plazas, R., Montávez, J. P., Jerez, S., Gómez-Navarro, J. J., Jiménez-Guerrero, P., & Jiménez, P. A. (2015). A 49 year hindcast of surface winds over the Iberian Peninsula. Int. J. Climatol., 35(10), 3007–3023.

[13] Uppala, S. M. et al. (2005). The ERA-40 re-analysis. Q. J. R. Meteorol. Soc. 131(612), 2961–3012.

[14] Costas, S., Jerez, S., Trigo, R. M., Goble, R., Rebêlo, L. (2012). Sand invasion along the Portuguese coast forced by westerly shifts during cold climate events. Quat. Sci. Rev. 42, 15–28.

[15] González-Villanueva, R., Costas, S., Pérez-Arlucea, M., Jerez, S., Trigo, R. M. (2013). Impact of atmospheric circulation patterns on coastal dune dynamics, NW Spain. Geomorphology, 185, 96–109.

[16] Jerez, S., Trigo, R. M., Vicente-Serrano, S. M., Pozo-Vázquez, D., Lorente-Plazas, R., Lorenzo-Lacruz, J., Santos-Alamillos, F., Montávez, J. P. (2013). The impact of the North Atlantic Oscillation on renewable energy resources in southwestern Europe. J. Appl. Meteorol. Climatol. 52(10), 2204–2225.

[17] Azorin-Molina, C., Vicente-Serrano, S. M., McVicar, T. R., Jerez, S., Sanchez-Lorenzo, A., López-Moreno, J. I., Revuelto, J., Trigo, R.M., Lopez-Bustins, J.A., Espírito-Santo, F. (2014). Homogenization and Assessment of Observed Near-Surface Wind Speed Trends over Spain and Portugal, 1961–2011. J. Clim.27(10), 3692–3712.

[18] Azorin-Molina, C., Guijarro, J. A., McVicar, T. R., Vicente-Serrano, S. M., Chen, D., Jerez, S., Espírito-Santo, F. (2016). Trends of daily peak wind gusts in Spain and Portugal. J. Geophys. Res. (D Atmos.) 1961–2014.

[19] Hernández, A., Trigo, R. M., Pla-Rabes, S., Valero-Garcés, B. L., Jerez, S., Rico-Herrero, M., Vega, J.C., Jambrina-Enríquez, M., Giralt, S. (2015). Sensitivity of two Iberian lakes to North Atlantic atmospheric circulation modes. Clim. Dyn. 45(11–12), 3403–3417.

[20] Lorente-Plazas, R., Montávez, J. P., Jerez, S., Gómez-Navarro, J. J., Jiménez-Guerrero, P., & Jiménez, P. A. (2015). A 49 year hindcast of surface winds over the Iberian Peninsula. Int. J. Climatol. 35(10), 3007–3023.

[21] Paulson, C.A. (1970). The mathematical representation of wind speed and temperature profiles in the unstable atmospheric surface layer. J. Appl. Meteorol. 9: 857-861.

[22] Sanz Rodrigo, J., Cantero, E., Garcia, B., Borbón, F., Urigoyen, U., Lozano, S., Fernandes, P.M., Chávez, R.A. (2015). Atmospheric stability assessment for the characterization of offshore wind conditions. J. Phys: Conf. Ser. 625 012044.

[23] Hsu, S.A., Meindl, E.A., Gilhousen, D.B., 1994. Determining the Power-Law Wind-Profile Exponent under Near-Neutral Stability Conditions at Sea. J. Appl. Meteorol. 33: 757–765.

[24] Gryning, S.E., Batchvarova, E., Brummer, B., Jørgensen, H., Larsen, S. (2007). On the extension of the wind profile over homogeneous terrain beyond the surface boundary layer. Boundary-Layer Meteorol. 124: 251–268.

[25] Schwartz, M., Heimiller, D., Haymes, S., Musial, W. (2010). Assessment of Offshore Wind Energy Resources for the United States. US National Renewable Energy Laboratory. Technical Report NREL/TP-500-45889, 104 pp.

[26] Elliott, D., Holliday, C., Barchet, W., Foote, H., Sandusky, W. (1987). Wind Energy Resource Atlas of the United States. DOE/CH 10093-4, Golden, Colorado: Solar Energy Research Institute.

[27] Salvação, N., Guedes Soares, C., Bentamy, A. (2015). Offshore wind energy assessment for the Iberian coasts using remotely sensed data. Renewable Energies Offshore – Guedes Soares (Ed.). Taylor & Francis: 237–244.

[28] Justus, C.G., Hargraves, W.R., Yalcin, A. (1976). Nationwide assessment of potential output from wind powered generators. J. Appl. Meteorol. 15: 673–678.

[29] Seguro, J.V., Lambert, T.W. (2000). Modern estimation of the parameters of the Weibull wind speed distribution for wind energy analysis. J. Wind Eng. Ind. Aerodyn. 85(1): 75–84.

[30] Stevens, M.J., Smulders, P.T. (1979). The estimation of the parameters of the Weibull wind speed distribution for wind energy utilization purposes, Wind Eng. 3(2): 132–145.

[31] Staffel, I., Pferringen, S. (2016). Using bias-corrected reanalysis to simulate current and future wind power output. Energy 114: 1224-1239.

[32] Andresen, G.B., Søndergaard, A.A., Greiner, M. (2015). Validation of Danish wind time series from a new global renewable energy atlas for energy system analysis. Energy 93(1): 1074-1088.

[33] Huber, M., Dimkova, D., Hamacher, T. (2014). Integration of wind and solar power in Europe: Assessment of flexibility requirements. Energy 69(1): 236-246.

[34] Marujo, R., Costa, P., Couto, A., Simões, T., Estanqueiro, A. (2013). Offshore Wind Resource Assessment Portuguese Atlantic Coast, AEP estimation in the regions of Viana do Castelo, Peniche and S. Pedro de Moel (Pilot Zone). Final report Laboratório Nacional de Energia e Geologia, 36 pp.

[35] Jesus, F., Menéndez, M., Guanche, R., Losada, I.J. (2014). A wind chart to characterize potential offshore wind energy sites. Computers & geosciences 71, 62–72.

[36] Castro-Santos, L., Diaz-Casas, V. (2016). Floating Offshore Wind Farms. Green Energy and Technology, Springer, 204 pp.

[37] Robertson, A.N., Jonkman, J.M., Goupee, A.J., Coulling, A.J., Prowell, I., Browning, J., Masciola, M.D., Molta, P. (2013) Summary of conclusions and recommendations drawn from the DeepCWind scaled floating offshore wind system test campaign. In: ASME 2013 32nd international conference on ocean, offshore and arctic engineering. American Society of Mechanical Engineers, V008T09A053-V008T09A053.

[38] Nihei Y, Iijima K, Murai M, Ikoma T (2014) A comparative study of motion performance of four different FOWT designs in combined wind and wave loads. In: ASME 2014 33rd international conference on ocean, offshore and arctic engineering. American Society of Mechanical Engineers, V007T05A025-V007T05A025.

FIGURE CAPTIONS

Figure 1. Existing offshore wind technology concepts and depth ranges.

Figure 2. Illustration of the various metocean factors influencing a floating offshore wind turbine (adapted from the US National Renewable Energy Laboratory).

Figure 3. The Sagres Area, SW coast of Portugal.

Figure 4. (A) Theoretical wind power time series (Wm^{-2}) at a height of 80 m (with $\alpha = 0.1$); (B) Weibull probability density function adapted to the model data; (C) Boxplot of the monthly wind speed distribution; (D) Wind rose at the APLF site constructed from the hindcast 49 year data set.

Figure 5. (A) Wind power time series (Wm^{-2}) from the in situ 80 m mast velocity measurements located inside the APLF; (B) Weibull probability density function adapted to the observed in situ data; (C) Boxplot of the monthly wind speed distribution; (D) Wind rose at the APLF site extracted from the directional sensor.

Figure 6. (A) Weibull probability density function obtained using the hindcast data for a height of 80 m 5 NM offshore the APLF (using $\alpha = 0.05$); (B) Weibull cumulative distribution function representing the mean regime; (C) Boxplot of the monthly wind speed distribution; (D) Wind rose at 5 NM offshore.

Figure 7. (A) Weibull probability density function obtained using the hindcast data for a height of 80 m 10 NM offshore the APLF (using $\alpha = 0.05$); (B) Weibull cumulative distribution function representing the mean regime; (C) Boxplot of the monthly wind speed distribution; (D) Wind rose at 10 NM offshore.

Figure 8. (A1–D1) Weibull PDF and (A2–D2) CDF at 5 NM and 10 NM offshore for z = 66 m, z = 88 m, z = 90 m, and z = 95 m hub heights, respectively, and (A3–D3) power curves for the four turbine devices evaluated in this study.

TABLE CAPTIONS

Table 1. Advantages and disadvantages of different offshore wind technology concepts, technology readiness level (TRL), and the major device manufacturers.

Table 2. Characteristics of four different turbines normally used in offshore wind farms.

Table 3. In situ data coverage from the meteorological station located in the Aeolian Park of Lagoa Funda (APLF) and used for validating the hindcast model.

Table 4. Weibull PDF parameters for the APLF onshore site and for the 5 NM and 10 NM offshore sites.

Table 5. Power density, energy output production, coefficient factors, and full load hours for four aero generators hypothetically placed at 5 NM and 10 NM offshore.

Table 6. Wind power classes defined by the US National Renewable Energy Laboratory as a function of power density and wind speed at different heights.

FIGURE 1

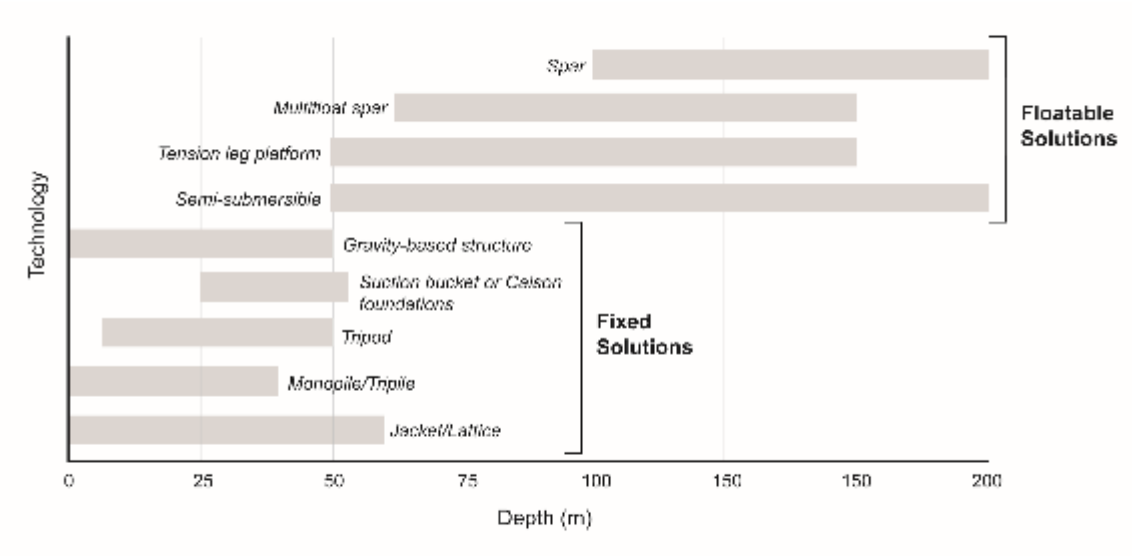
Spar
Multifloat spar
Tension leg platform
Semi-submersible
Gravity-based structure
Suction bucket or Caison foundations
Tripod
Monopile/Tripile
Jacket/Lattice
Floatable Solutions
Fixed Solutions
Technology
0
25
50
75
100
150
150
200
Depth (m)

FIGURE 2

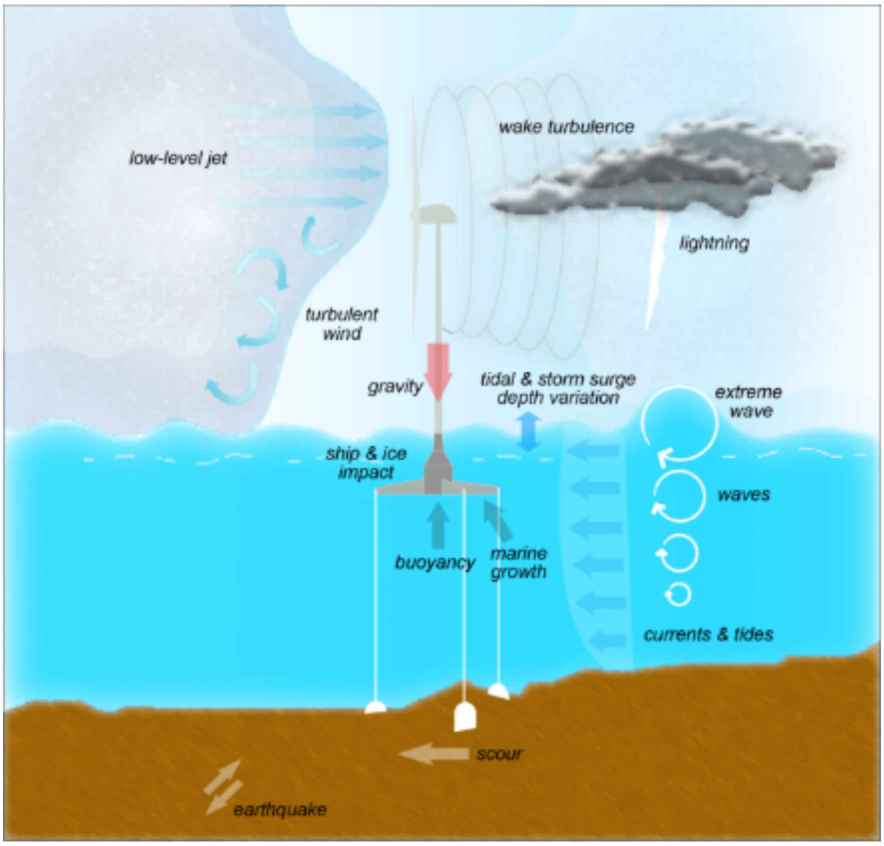
low-level jet
wake turbulence
lightning
turbulent wind
gravity
tidal & storm surge depth variation
extreme wave
ship & ice impact
waves
buoyancy
marine growth
currents & tides
scour
earthquake

FIGURE 3


N
W
E
S
SINES
VILA NOVA
MILFONTES
ODEMIRA
Atlantic Ocean
ALJEZUR
LAGOS
VILA DO BISPO
Cape St. Vicente
SAGRES
100m
200m
500m
10 km
SPAIN
PORTUGAL
Port of Sines
Sines Wave buoy
Aeolian Park
Lagoa Funda (APLF)

FIGURE 4

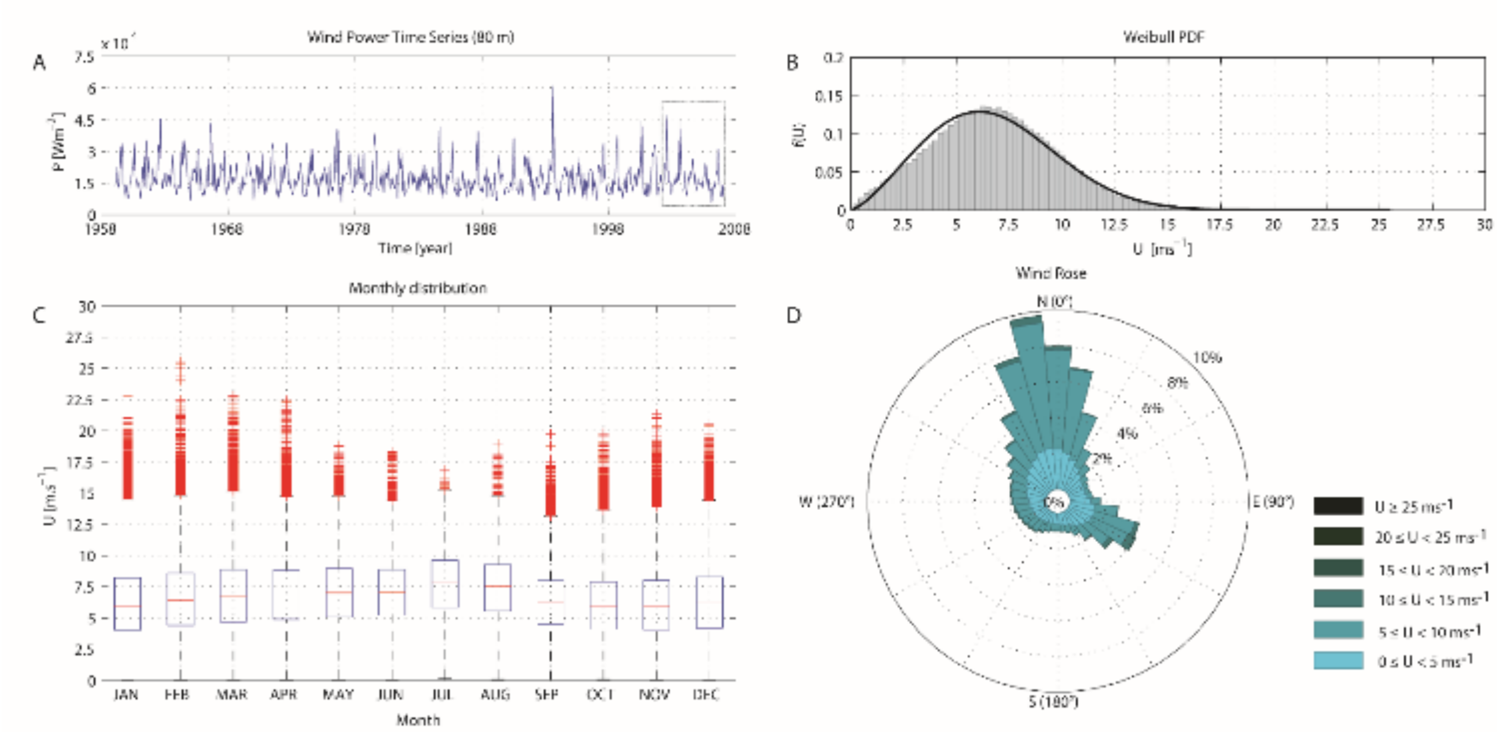
A
Wind Power Time Series (80 m)
P [Wm⁻²]
Time [year]
B
Weibull PDF
f(U)
U [ms⁻¹]
C
Monthly distribution
U [m.s⁻¹]
JAN
FEB
MAR
APR
MAY
JUN
JUL
AUG
SEP
OCT
NOV
DEC
Month
D
Wind Rose
N (0°)
E (90°)
S (180°)
W (270°)
10%
8%
6%
4%
2%
0%
U ≥ 25 ms⁻¹
20 ≤ U < 25 ms⁻¹
15 ≤ U < 20 ms⁻¹
10 ≤ U < 15 ms⁻¹
5 ≤ U < 10 ms⁻¹
0 ≤ U < 5 ms⁻¹

FIGURE 5

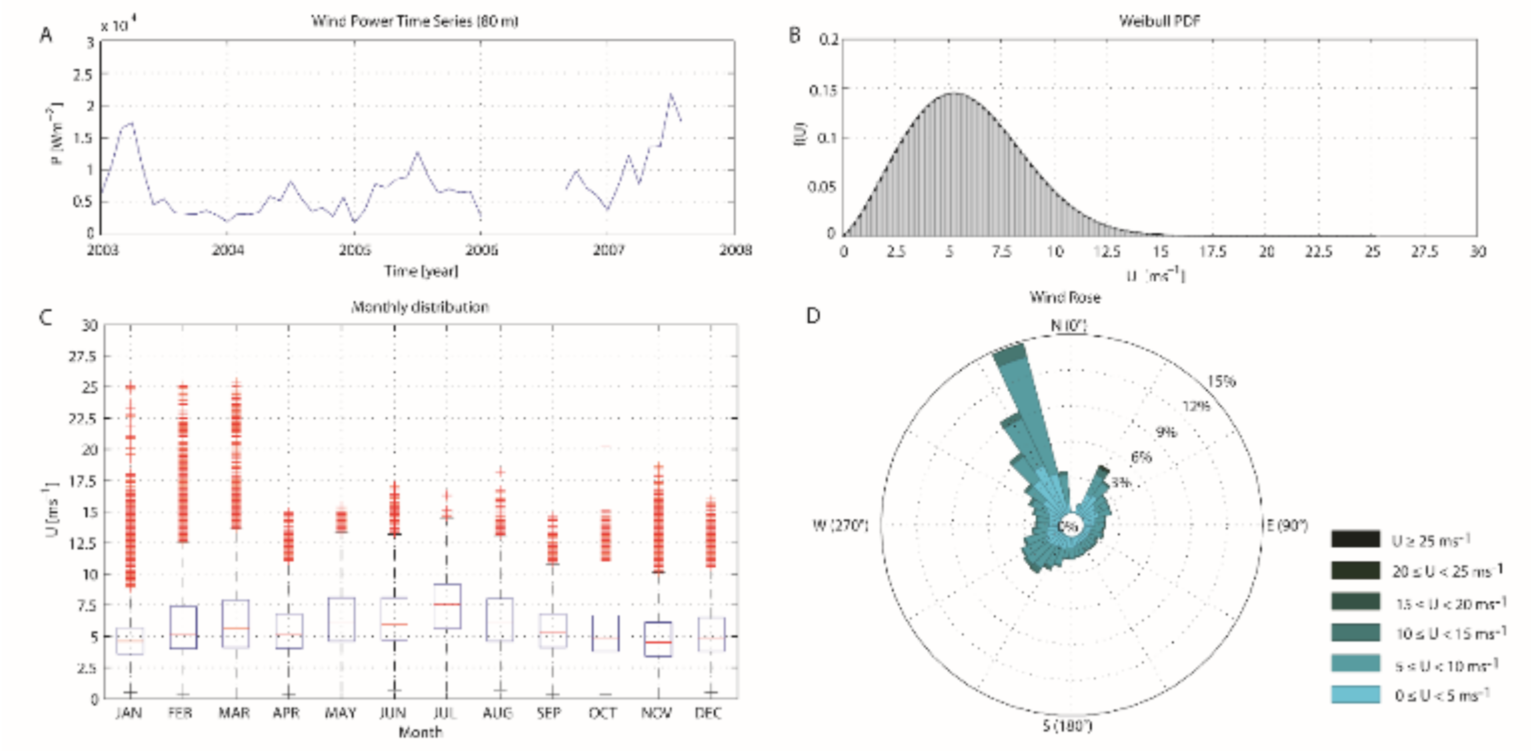
A
Wind Power Time Series (80 m)
P [Wm⁻²]
Time [year]
B
Weibull PDF
f(U)
U [ms⁻¹]
C
Monthly distribution
U [ms⁻¹]
JAN FEB MAR APR MAY JUN JUL AUG SEP OCT NOV DEC
Month
D
Wind Rose
N (0°)
E (90°)
S (180°)
W (270°)
U ≥ 25 ms⁻¹
20 ≤ U < 25 ms⁻¹
15 ≤ U < 20 ms⁻¹
10 ≤ U < 15 ms⁻¹
5 ≤ U < 10 ms⁻¹
0 ≤ U < 5 ms⁻¹

FIGURE 6

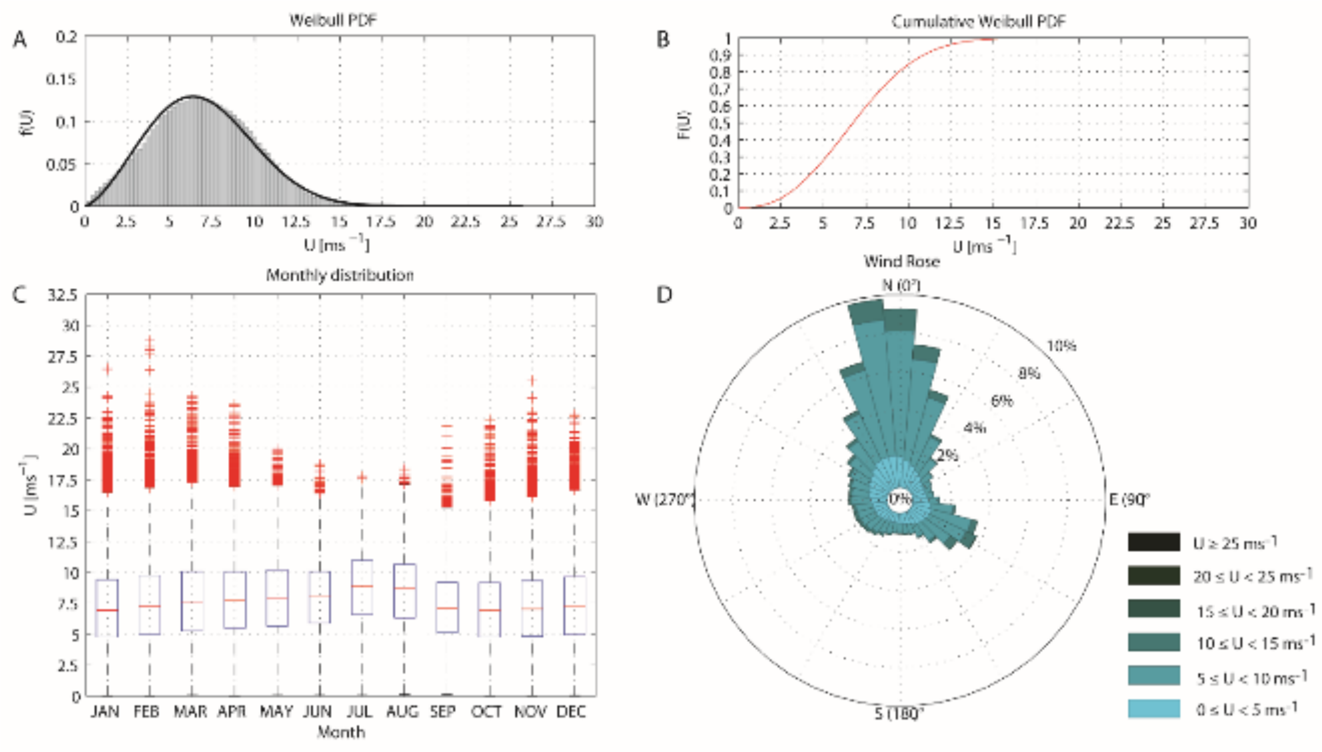
A
Weibull PDF
f(U)
U [ms⁻¹]
B
Cumulative Weibull PDF
F(U)
U [ms⁻¹]
C
Monthly distribution
U [ms⁻¹]
JAN FEB MAR APR MAY JUN JUL AUG SEP OCT NOV DEC
Month
D
Wind Rose
N (0°)
E (90°)
S (180°)
W (270°)
0%
2%
4%
6%
8%
10%
U ≥ 25 ms⁻¹
20 ≤ U < 25 ms⁻¹
15 ≤ U < 20 ms⁻¹
10 ≤ U < 15 ms⁻¹
5 ≤ U < 10 ms⁻¹
0 ≤ U < 5 ms⁻¹

FIGURE 7

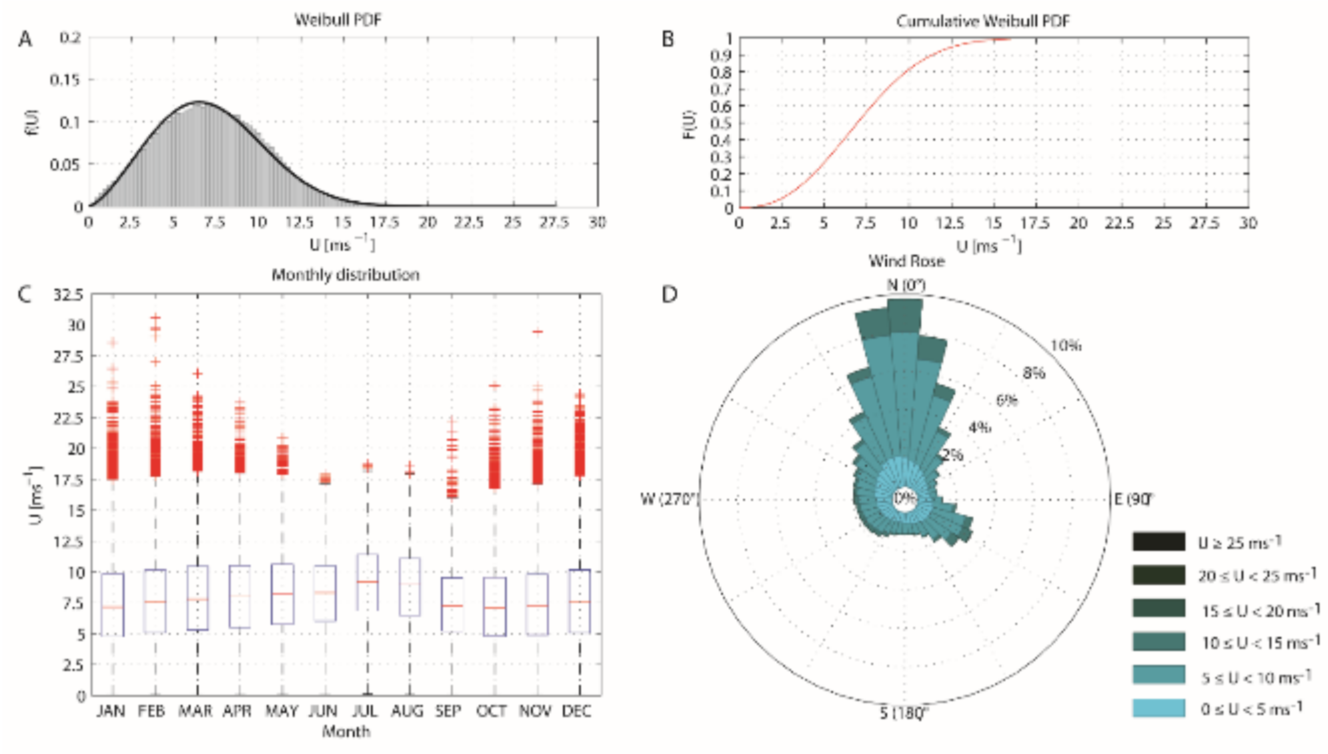
A
Weibull PDF
f(U)
U [ms⁻¹]
B
Cumulative Weibull PDF
F(U)
U [ms⁻¹]
C
Monthly distribution
U [ms⁻¹]
JAN FEB MAR APR MAY JUN JUL AUG SEP OCT NOV DEC
Month
D
Wind Rose
N (0°)
E (90°)
S (180°)
W (270°)
0% 2% 4% 6% 8% 10%
U ≥ 25 ms⁻¹
20 ≤ U < 25 ms⁻¹
15 ≤ U < 20 ms⁻¹
10 ≤ U < 15 ms⁻¹
5 ≤ U < 10 ms⁻¹
0 ≤ U < 5 ms⁻¹

FIGURE 8

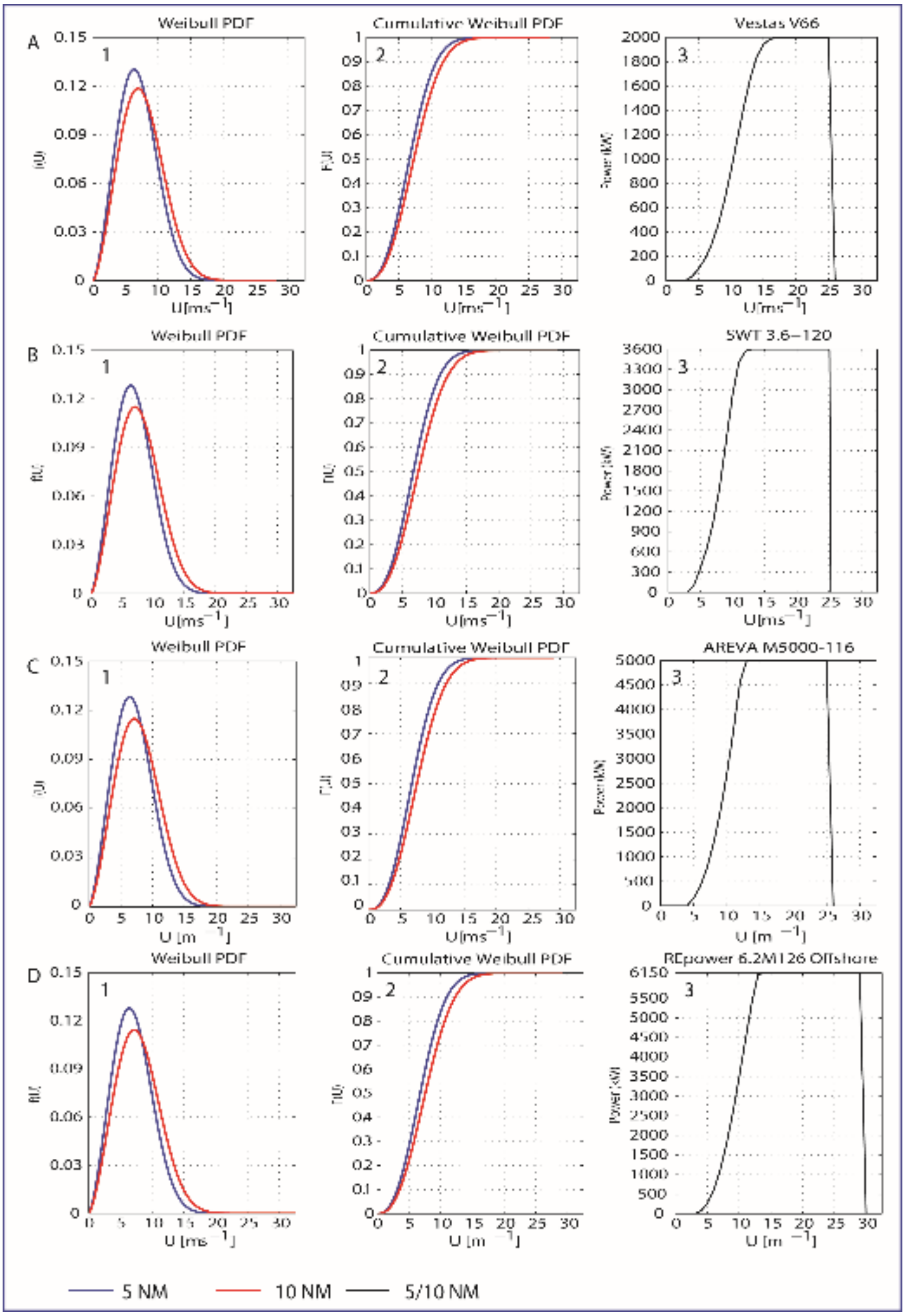
A
B
C
D
Weibull PDF
Cumulative Weibull PDF
Vestas V66
SWT 3.6–120
AREVA M5000-116
REpower 6.2M126 Offshore
f(U)
F(U)
Power [kW]
U[ms⁻¹]
5 NM
10 NM
5/10 NM

TABLE 1

Type	Pros	Cons	Concept	Depth range [m]	TRL	Pros	Cons	Technology examples
Fixed	Reduced costs in O&M costs; Shorter grid lines to shore.	Some concepts are affected by scouring; Sea-bed characteristics represent an important constraint; Impact on the coastal landscape; Expensive installation process.	Jacket/Lattice	0-60	9	Good stability; Foundations are lighter, therefore making installation easier Fabrication expertise is widely available, in part due to Offshore Oil and Gas industry supply chain.	High initial construction costs and potentially higher maintenance costs; Transportation is moderately difficult and expensive.	Quattropod® (by OWEC Tower AS - NO); Hochtief Solutions AG (DE); ATKINS/BIFab Jacket (UK); Twisted Jacket Foundation (by Keystone Engin. Inc - USA)
			Monopile	0-40	9	Simple, versatile; Suitable for most soil conditions other than deep soft material; Minimum footprint.	Very expensive installation; Difficult to remove; More susceptible to scour; Performance can be limited due to resonance effects.	LICengineering A/S (DK)
			Tripod	6-50	9	Good stability and overall stiffness; Minimum preparation of the sea-floor prior to installation.	Not suited for locations with uneven sea beds with large boulders; Potential greater risk of fatigue from the large impact of wind and waves; Expensive at greater depths; More corrosion than monopiles.	Weserwind tripods (DE)
			Tripile	0-40	9	Simplicity of their design; Improved stiffness; Automated leveling process.	Requires large amounts of materials; Manufacturing is labour intensive.	Triple (by BARD Engineering GmbH - DE)
			Suction Bucket or Caisson Foundations	25-65	9	Lightweight structure; Only requires a single operation during deployment.	Installation proven in limited range of sea-floor properties.	Mono bucket (by Universal Foundation - DK); Suction bucket (by LICengineering - DK)
			Gravity Based Structure (GBS)	0-50	9	Float out Installation; Improved performance against structural flexibility.	Costs increase rapidly with water depth; Wide footprint.	Cranefree Gravity® (by SeaTower); Gravitas Gravity Base (by Arup/Costain/Hochtief)
Floatable	Access to a greater wind resource; Wind turbines can be installed quayside before towing; Lower environmental impact on coastal landscape; Decommissioning without any component left on the sites.	Operation and maintenance costs are higher (greater distance to port); More expensive designs to sustain harsh environments; Preventing dynamic motion of the floatable structure increases costs.	Floating	30-150	8	Shallow draft.	Unacceptable motion in waves.	Damping Pool® (by IDEOL - FR)
			Semi-submersible	40-1000	8	Low motions in waves.	Platform needs to be large to achieve required stability.	WindFloat (by Principle Power Inc - USA); Sea-Reed (by DCNS - FR); WinFlo (by DCNS - FR); V-Shape (by Mitsubishi Heavy industries Ltd. - JP)
			Spar	100-200	8	Low motions in waves.	Very deep draft.	Hywind (by Statoil - NO); SWAY® (by Sway - NO); Advanced Spar (by Japan Marine United Corp. – JP)
			Multifloat-spar	65-150	3	Low motions in waves; Shallower draft than Spar.	Only at TRL 3.	Starfloat (by Oceanflow Energy Development - GB)
			Tension Leg Platform (TLP)	60-160	8	Very low motion; Small structure.	Difficult and expensive to install and fit out with turbine.	PelaStar (by Glosten Associates - USA); Gicon® SOF (by GICON Holding GmbH DE); Blue H (NL)

TABLE 2

Parameter	TURBINE			
	Vestas V66	**SWT 3.6-120**	**AREVA M5000-116**	**REpower 6.2M126 Offshore**
Rated capacity (kW)	2000	3600	5000	6150
Cut-in speed (m/s)	4	3.5	4	3.5
Rated wind speed (m/s)	17	12	12.5	14
Cut-out speed (m/s)	25	25	25	30
Rotor diameter (m)	66	120	116	126
Hub height (m)	66	88	90	95
Swept area (m^2)	3421	11300	10568	12469
No. blades	3	3	3	3
Tip speed (m/s)	68.4	81.7	89.9	95
Generator type	Induction with optispeed	Asynchronous	Synchronous permanent	Double Fed Asyn
Manufacturer	Vestas Wind Systems A/S	Siemens	AREVA Wind GmbH	REpower Systems SE
Country	Denmark	Germany	Germany	Germany

TABLE 3

	JAN	FEV	MAR	APR	MAY	JUN	JUL	AGO	SEP	NOV	DEC
2003											
2004											
2005											
2006											
2007											

Note: Black cells mean a total absence of data; grey cells mean <75% of data coverage.

TABLE 4

Site	U_{mean} (ms^{-1})	σ (ms^{-1})	U_{max} (ms^{-1})	k	c (ms^{-1})
APLF_MODEL*	6.74	2.98	25.56	2.39	7.59
APLF_STATION	5.91	2.63	25.40	2.36	6.70
APLF_MODEL^{+}	6.08	2.68	23.04	2.39	6.84
Offshore					
5 NM^{+}	6.94	2.97	25.90	2.49	7.81
10 NM^{+}	7.18	3.12	27.56	2.45	8.09

*** Equation 3 with $\alpha = 0.1$; $^{+}$ Equation 3 with $\alpha = 0.05$**

TABLE 5

Model	Rotor ∅ (m)	A_T (m^2)	Site	P (MW)	U_{mean} (ms^{-1})	σ (ms^{-1})	U_{max} (ms^{-1})	k	c (ms^{-1})	P_{mean} (kW)	E_{out} (kWhyear^{-1})	C_F	Full load hours	P_{out} (W m^{-2})
Vestas V66	66	3421	5 NM	959	6.87	2.94	25.65	2.49	7.73	4.20E+02	3.68E+06	0.21	1837	123
			10 NM	1158	7.55	3.23	28.19	2.49	8.49	5.33E+02	4.67E+06	0.27	2336	156
SWT 3.6-120	120	11300	5 NM	987	6.97	2.98	26.02	2.49	7.84	1.30E+03	1.14E+07	0.36	3154	115
			10 NM	1226	7.77	3.32	29.01	2.49	8.74	1.60E+03	1.40E+07	0.45	3900	142
Areva M5000-116	116	10568	5 NM	989	6.98	2.98	26.05	2.49	7.85	1.24E+03	1.09E+07	0.25	2174	117
			10 NM	1232	7.79	3.33	29.08	2.49	8.76	1.64E+03	1.44E+07	0.33	2872	155
REpower 6.2M 126 Offshore	126	12469	5 NM	994	7.00	2.99	26.12	2.49	7.87	1.62E+03	1.42E+07	0.26	2314	130
			10 NM	1245	7.83	3.35	29.24	2.49	8.81	2.12E+03	1.86E+07	0.34	3019	170

TABLE 6

Wind Power Class	At a height of 10 m *		At a height of 66 m		At a height of 90 m	
	Wind Power Density [Wm^{-2}]	Speed [ms^{-1}] **	Wind Power Density [Wm^{-2}]	Speed [ms^{-1}] ($\alpha = 0.05$)	Wind Power Density [Wm^{-2}]	Speed [ms^{-1}] ($\alpha = 0.05$)
1	0–100	0– 4.4	0–130	0–4.8	0–140	0–4.9
2	100–150	4.4–5.2	130–200	4.8–5.6	140–215	4.9–5.7
3	150–200	5.2–5.6	200–275	5.6–6.2	215–285	5.7–6.3
4	200–250	5.6–6.0	275–335	6.2–6.6	285–350	6.3–6.7
5	250–300	6.0–6.4	335–400	6.6–7.0	350–425	6.7–7.2
6	300–400	6.4–7.0	400–535	7.0–7.7	425–550	7.2–7.8
7	400–1000	7.0–9.4	535–1300	7.7–10.3	550–1350	7.8–10.5

* Vertical extrapolation of wind speed based on the power law with $\alpha = 0.05$. ** Mean wind speed is based on a Rayleigh speed distribution of equivalent mean wind power density ($P_{avg} = 0.955*\rho*U^3$). Wind speed is for standard sea-level conditions. To maintain the same power density, wind speed increases by 3%/1000 m elevation.